Continuous synthesis of menthol from citronellal and citral over Ni-beta-zeolite-sepiolite composite catalyst

Simakova, Irina; Mäki-Arvela, Päivi; Martinez-Klimov, Mark; Muller, Joseph; Vajglova, Zuzana; Peurla, Markus; Eränen, Kari; Murzin, Dmitry Yu

Continuous synthesis of menthol from citronellal and citral over Ni-beta-zeolite-sepiolite composite catalyst

Irina Simakova [a], Päivi Mäki-Arvela [b], Mark Martinez-Klimov [b], Joseph Muller [b], Zuzana Vajglova [b], Markus Peurla [c], Kari Eränen [b], Dmitry Yu. Murzin [b,*]

[a] *Boreskov Institute of Catalysis, pr. Ak. Lavrentieva 5, 630090, Novosibirsk, Russia*
[b] *Åbo Akademi University, Johan Gadolin Process Chemistry Centre, Henriksgatan 2, 20500, Turku/Åbo, Finland*
[c] *Institute of Biomedicine, University of Turku, Kiinamyllynkatu 10, FI-20520 Turku, Finland*

ABSTRACT

One-pot continuous synthesis of menthols both from citronellal and citral was investigated over 5 wt% Ni supported on H-Beta-38-sepiolite composite catalyst at 60–70 °C under 10–29 bar hydrogen pressure. A relatively high menthols yield of 53% and 49% and stereoselectivity to menthol of 71–76% and 72–74% were obtained from citronellal and citral respectively at the contact time 4.2 min, 70 °C and 20 bar. Citral conversion noticeably decreased with time-on-stream under 10 and 15 bar of hydrogen pressure accompanied by accumulation of citronellal, the primary hydrogenation product of citral, practically not affecting selectivity to menthol. A substantial amount of defuctionalization products observed during citral conversion, especially at the beginning of the reaction (ca. 1 h), indicated that all intermediates could contribute to formation of menthanes. Ni/H-Beta-38-sepiolite composite material prepared by extrusion was characterized by TEM, SEM, XPS, XRD, ICP-OES, N_2 physisorption and FTIR techniques to perceive the interrelation between the physico-chemical and catalytic properties.

1. Introduction

Naturally occurring (−)-menthol, that can be obtained by distillation of essential oils, has a wide application in cosmetic, pharmaceutical and fragrance industries because of its organoleptic properties and special menthe odour. Since 1980 s the enantioselective menthol synthesis from myrcene was realized industrially by Takasago process using $ZnBr_2$, H_2SO_4 and Rh-organometallic compounds as homogeneous catalysts considered, however, as rather hazardous ones for the environment [1]. Menthol synthesis from piperitone as a starting reagent over homogeneous catalyst has been also reported [2]. Citral is present naturally in the essential oils and can be extracted from different plants, such as lemon myrtle (90–98%), Litsea citrata (90%), Litsea cubeba (70–85%), lemongrass (65–85%), lemon tea-tree (70–80%) and many others [3]. It worth to note that citral has been manufactured industrially from cheap multi-tonnage feedstock- isobutene and formaldehyde [4] addressing an increased demand in citral for the synthesis of carotenoids, vitamins A, E and a range of aroma chemicals.

One-pot synthesis of menthol starting from an available renewable source (citral) over heterogeneous catalysts (Fig. 1) is highly interesting.

An alternative method to produce menthol is to apply a two-step method starting from citronellal isomerization to isopulegol [5–7] followed by its hydrogenation to menthol [8]. The first step of citronellal isomerization requires an acidic catalyst [6], while the metal is needed for hydrogenation of isopulegol [5]. The benefit of heterogeneous catalysts is their easy separation and reuse, as well as lower prices, especially when nonprecious transition metal supported catalysts are applied. One-pot synthesis of menthol from citronellal both in batch [9–23] and continuous operations [24–26] has already been intensively studied. However, the majority of one-pot citral transformations has been performed in batch reactors using different supported Ni, Cu, Pd, Ru, Rh, Ir, Pt metal catalysts [27–34]. Application of a bifunctional catalyst for citral transformations to menthol is a promising way comprising hydrogenation of citral to citronellal followed by ene-cyclisation of the intermediate citronellal into isopulegol as well as hydrogenation of isopulegol to menthol in one-step. One of the challenges is to avoid consecutive over-hydrogenation of citronellal to citronellol and then to 3,7-dimethyloctanol as well as

defunctionalization of reaction intermediates at each step. To avoid over-hydrogenation, for example, Adilina et al. [9] carried out cyclization of (±)-citronellal to (±)-isopulegol under air stirring the mixture at 70 ºC followed by hydrogenation of isopulegol towards the desired (-)-menthol at 2 MPa of H_2 pressure. Ni on a natural zeolite as a catalyst was able to convert a (±)-citronellal derivative yielding 9% (-)-menthol (36% selectivity) with conversion up to 24%, whereas Ni on ZSM-5 directly converted 65% (±)-citronellal to give 4% menthol (6% selectivity) [9]. Among reported Ni containing catalysts the highest menthol yields were obtained from citral transformations at 70 °C under 2 MPa hydrogen over 8 wt% Ni/Al-H-MCM-41 [31] and 15 wt% Ni-MCM-41-Zr-Beta [31] (Table 1, entries 1,2) giving above 94% menthol yield. Over Pd/HBEA high amounts of acyclic hydrogenation products, especially 3,7-dimethyloctanal were also formed [27]. In the literature [33] the maximum yield of menthols was 54% over 5 wt% Ni-H-MCM-41 (Table 1, entry 3), while 3 wt% Ni-H-Beta gave 73% menthol yield (Table 1, entry 5) [27] demonstrating an important role of support acidity. The effect of metal loading in citral transformations was studied revealing that 8 wt% Ni was more efficient for producing menthol compared to 5 wt% Ni- heteropolyacid-montmorillonite (HPA-MM). The high menthol yield over 8 wt% Ni-HPA-MM was related to its low Brønsted to Lewis acid sites ratio [32]. Cu/sepiolite was also used as a catalyst in citral transformations to menthol in heptane at 90 °C under 1 bar hydrogen in a batch reactor giving 45% menthol yield in 55 h (Table 1, entry 7) [34]. Studying the effect of the metal nature Trasarti et al. noted that among silica supported noble (Pd, Pt, Ir) and non-noble (Co, Cu, Ni) metals a faster initial rate of citronellal formation from citral was observed on Pd and Ni [31]. This can be explained by a narrower D-band width of Ni and Pd compared to other metals decreasing thereby the electrostatic repulsion between the metal and the conjugated C=C bond of citral. This leads to more prominent adsorption of citral via its C=C bond followed by concurrent hydrogenation to citronellal [31]. The menthol yield over 1%Pd/HBEA (HBEA - commercial zeolite, Zeo-cat PB) was only ca. 20% with a high amount of acyclic hydrogenation products, especially 3,7-dimethyloctanal, showing that bifunctional Pd/HBEA cannot selectively convert citral to menthols in an one-step process leading to over-hydrogenation [31].

A comparable study of the catalytic behaviour of Pd, Ru, Rh, Ir, Pt supported on Beta zeolites in one-pot citral hydrogenation in toluene reported that the menthol yield obtained at 100 °C under 1.0 MPa hydrogen in 24 h decreased in the following order: Pd (51.4%) > Ir (43.8%)> > Ru (9.6%) [30]. The solvent nature strongly affected the menthol yield as was shown for 3% Pd/Beta [30], namely the highest menthol yields were found for citral hydrogenation in ethylene glycol

(65.8%) and 2-methyl-THF (78.6%) (Table 1, entry 8) [30]. No menthols were formed over Rh/Beta and Pt/Beta, whereas a high amount of dehydration products was generated over these catalysts [30]. Pd supported together with $ZnCl_2$ and *n*-butyl-4-methylpyridinium tetrafluoroborate ionic liquid on an active carbon cloth gave 40% menthol and ca. 35% 3,7-dimethyloctanal in one-pot citral transformations (Table 1, entry 9) [35], reflecting too high hydrogenation activity. Citral hydrogenation process in a continuous mode has been barely investigated, though some research works, mainly using Pd catalysts, were reported resulting in formation of citronellal and its hydrogenated derivatives without any menthol [36]. In our previous studies continuous citral hydrogenation into menthol was investigated over mildly acidic mesoporous Ru/MCM-41 [37] and microporous Ru/H-Y-80 [38] catalysts giving low menthol formation with defunctionalized menthatrienes as the main products. It is worth to note that sepiolite, a natural mineral which has the following chemical structure $Si_{12}O_{30}Mg_8(OH)_4(OH_2)_4 \cdot 8H_2O$ [39], was successfully used as a support for copper and this resulting catalyst was applied for synthesis of menthol in a batch reactor [34].

Analysis of the literature shows that Ni supported on zeolites could be a very efficient catalyst in one-pot menthol synthesis from citral and citronellal. To the best of our knowledge one-pot menthol synthesis with nickel catalysts starting from citral has been investigated only in our recent work in a continuous reactor using a mildly acidic 5 wt% Ni/MAS (mesoporous alumino silicate) as a catalyst [40], while transformations of citronellal to menthol in a continuous reactor using Ni supported catalysts have not been yet reported in the open literature.

In order to fill the obvious gap in this research area the aim of the current work is to investigate behavior of bifunctional Ni/H-Beta-38-sepiolite extruded catalyst in continuous one-pot synthesis of menthol from citronellal or citral and to correlate the catalytic results with the catalyst properties studied by TEM, SEM, XPS, XRD, N_2 physisorption and FTIR.

2. Experimental section

2.1. Catalyst preparation

Ni supported on (H-Beta-38 +sepiolite) extrudates were prepared using nickel nitrate $Ni(NO_3)_2 \cdot 6 H_2O$ (98%) (Sigma Aldrich, >97%) as a metal precursor, NH_4-Beta-38 (molar ratio of SiO_2/Al_2O_3 =38, CP814C, Zeolyst International) as a support, sepiolite ($Mg_2H_2SiO_9 \cdot 9 H_2O$, Sigma-Aldrich) as a mineral binder and methylcellulose (viscosity: 4000 cP, Sigma-Aldrich) as an organic binder.
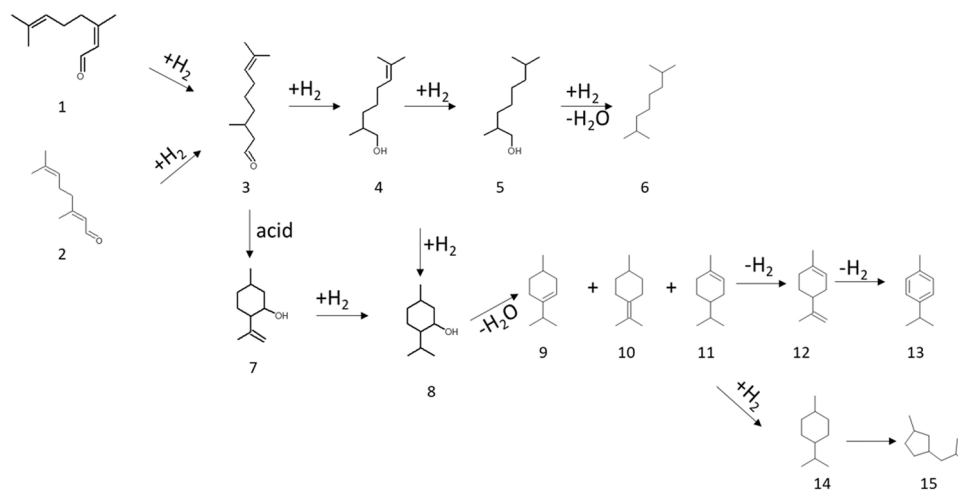

Fig. 1. Reaction scheme for citral transformations over bifunctional catalysts. Notation: 1. cis-citral, 2. trans- citral, 3. citronellal, 4. citronellol, 5. 3,7-dimethyloctanol, 6. 3,7-dimethyloctane, 7. pulegol, 8. menthol, 9. 3-menthene, 10. p-4(8)-menthene, 11. 1-menthene, 12. L-limonene, 13. p-cymene, 14. 1-methyl-4–1-methylethylmenthane, 15. 1-methyl-3–2-methylpropylcyclopentane.

Table 1
Citral transformations to menthols in a batch reactor and in this study in a continuous mode.

Entry	Catalyst	Conditions	Conversion (%)	Yield of menthols (%)	Stereoselectivity to (-)-menthol (%)	Ref.
1	8 wt% Ni-Al-MCM-41	Toluene, 2.0 MPa H_2, 70 °C, $c_0 = 0.18$ mol/l, $m_{cit}/m_{cat} = 1.7$ wt/wt, 6 h	100	94	71	31
2	15 wt% Ni-MCM-41-Zr-Beta	Tert-butanol, 0.2 MPa H_2, 80 °C, $c_0 = 0.20$ mol/l, $m_{cit}/m_{cat} = 5.1$ wt/wt, 8 h	100	95	89	29
3	5 wt% Ni-H-MCM-41	Cyclohexane, 0.1 MPa H_2, 70 °C, $c_0 = 0.01$ mol/l, $m_{cit}/m_{cat} = 1.0$ wt/wt, 330 min	100	54	73	33
4	8 wt% Ni-HPA-MM	cyclohexane, 1.0 MPa H_2, 80 °C, $c_0 = 0.18$ mol/l, $m_{cit}/m_{cat} = 3.4$ wt/wt, 30 h	100	63		32
5	3 wt% Ni-H-Beta	Toluene, 0.5 MPa H_2, 70 °C, $c_0 = 0.08$ mol/l, $m_{cit}/m_{cat} = 1.8$ wt/wt, 240 min	100	81	72	27
6	5 wt% Ni/MAS (mesoporous alumino silicate)	Cyclohexane, 10 bar, 70 °C, $c_0 = 0.086$ mol/l, contact time 4.2 min, residence time 16.7 min, time-on-stream 56 h	100 -> 54	75	72–76	40
7	5 wt% Ni/(H-Beta-38 +sepiolite)	Cyclohexane, 20 bar, 70 °C, $c_0 = 0.086$ mol/l, contact time 4.2 min, residence time 16.7 min, time-on-stream 180 min	88	49	72–74	This paper
8	Cu/Sepiolite	Toluene/heptane, 1 bar, 90 °C, $c_0 = 0.082$ mol/l, $m_{cit}/m_{cat} = 1.0$ wt/wt, 54 h	100	45	No data	34
9	3 wt% Pd/Beta	2-methyl-THF, 1.0 MPa H_2, 100 °C, $c_0 = 0.56$ mol/l, $m_{cit}/m_{cat} = 8.5$ wt/wt, 24 h	100	78.6	No data	30
10	Pd/ZnCl$_2$/NB4MPyBF$_4$/ACC	hexane, 0.5 MPa H_2, 100 °C, $c_0 = 0.08$ mol/l, 46 h	100	40	No data	35

The ammonium form of Beta-38 was transformed to H-Beta-38 by calcination increasing the temperature linearly to 250 °C, and thereafter to 400 °C [41].

H-Beta-38 zeolite and sepiolite were grinded (<63 μm), dried overnight at 100 °C and mixed as dry powders in the mass ratio = 70/30, e.g. 4.2 g and 1.8 g, respectively. Methylcellulose (1.0 wt% of the dry mixture weight, e.g. 0.06 g) was dissolved in 3 mL water and added into this mixture to control the rheological properties of the final slurry. Distilled water was added gradually into the suspension under constant stirring at a room temperature. The extrudates of the cylindrical shape and a diameter of 1.5 mm were prepared with a one-screw extrusion device (TBL-2, Tianjin Tianda Beiyang Chemical Co. Ltd., China) at the rotational velocity of 1400 rpm. Subsequently, the metal-free extrudates were dried in an oven at 100 °C overnight, calcined at 500 °C for 4 h in a muffle oven, and cut to a length of ca. 0.6–1.0 cm. The extrudates were then impregnated by the incipient wetness method with a nickel nitrate $Ni(NO_3)_2 * 6 H_2O$ aqueous solution to achieve the nominal nickel loading of 5 wt%. Thereafter Ni-bearing extrudates were dried overnight at 100 °C followed by calcination at 450 °C for 6 h in a muffle oven.

2.2. Catalyst characterization

The specific surface area and pore size distribution were determined by nitrogen physisorption using Micromeritics 3Flex-3500 surface characterization. Prior to the measurement the catalyst was evacuated at 150–200 °C overnight in an external device and at ca. 150–200 °C for 3–5 h below 8 mbar. The specific surface area was calculated using BET and Dubinin-Radushkevich methods and the non-local density functional method (NLDFT) was used for the pore size distribution. The latter method became recently one of the most widely used methods for determination of the pore size distribution and is recommended by IUPAC for this purpose [42].

The nickel particle size and the catalyst structure were analyzed by transmission electron microscopy (TEM) performed with a JEOL 2010 microscope. Before TEM measurements, a sample was dispersed in isopropanol and dropped on a copper grid coated with a carbon film. The metal particle sizes were determined from the TEM image using the software ImageJ. To estimate the value of a mean diameter of Ni nanoparticles more than 200 particles were counted. The catalyst morphology was also studied via performing scanning electron microscopy measurements using Zeiss Leo Gemini 1530 apparatus.

Elucidation of the phase purity and the crystal phase identification of Ni/(H-Beta-38 +sepiolite) crushed extrudates was performed by the powder X-ray diffraction (XRD) applying the Bragg-Brentano focusing

configuration. XRD patterns of the samples were recorded on X-ray diffractometer D8 Advance (Bruker, Germany) using CuKα radiation (λ = 1.5418 Å) and one-dimensional LynxEye detector with an angular range of 2.9° on the 2θ scale by scanning in the 2θ-angle range from 15° to 70° with a step of 0.05° and acquisition time of 3 s at each point. The sizes of the coherently scattering domains (CSD - DXRD) were determined from the broadening of diffraction peaks. The instrumental broadening of the diffraction lines was taken into account, which was recorded from the diffraction pattern of the standard α-Al$_2$O$_3$ (SRM 1976).

Fourier transform infrared spectroscopy of adsorbed pyridine (pyridine-FTIR) was performed using an ATI Mattson instrument to quantify Brønsted and Lewis acid sites. A thin self-supported catalyst wafer (10–20 mg) was pressed and placed in the FTIR cell, which was evacuated followed by heating to 450 °C under vacuum for 1 h. The background spectrum was measured at 100 °C. Pyridine (Sigma-Aldrich, >99.5%) was adsorbed on the sample for 30 min at 100 °C followed by its desorption at 250 °C, 350 °C, and 450 °C for 1 h to determine the weak, medium and strong acid sites. The spectra of the catalysts were recorded at 100 °C. Brønsted- and Lewis-acid sites were quantified using the spectral bands at 1545 and 1450 cm^{-1}, respectively and the amount of acid sites was quantified using the molar extinction coefficients of Emeis [43].

Elemental analysis of the fresh and spent catalysts was performed with inductively coupled plasma-optical emission spectroscopy (ICP-OES) using Perkin-Elmer Optima 5300 DV.

2.3. Catalytic experiments

Citronellal (Sigma Aldrich, ≥95.0 wt%) and citral (Sigma-Aldrich, *cis-/trans*-isomer ~ 1/1, ≥ 95.0%) transformations were investigated in a trickle bed reactor (the tube diameter 1.25 cm), in which both liquid and gas were flowing from top to bottom in a co-current mode. The liquid flow which rate was varied from 0.2 to 0.3 mL/min contained 0.086 mol/l citronellal or citral in cyclohexane. The hydrogen (AGA, 99.999%) flow rate was 150 mL/min at the total pressure of 20 bar, while with 10 and 15 bar it was 100 mL/min. The experiments were performed as follows: 5 wt% Ni/(H-Beta-38 +sepiolite) extrudates (1 g) with the length varying from 0.6 to 1.0 cm and the diameter of 1.5 mm were loaded together with 15 g of inert quartz of the size 0.2–0.8 mm. Prior to the reaction, the catalyst was reduced in situ using the following temperature program: 2 °C/min – 350 °C (120 min). The reaction temperature was set to 70 °C and the pressure was adjusted to 20 bar. The reaction was started when the cyclohexane was first pumped though the

catalyst bed in order to wet it. Thereafter, the liquid flow was changed to the feed flow. The contact time was varied in the range of 3.2–6.4 min corresponding to the residence times of 11.5–23 min. The liquid residence time was 16.7 min. After 180 min TOS, the pressure was adjusted first to 15 bar and finally after 5 h TOS to 10 bar. The total time-on-stream was 7 h. The reduced fresh catalyst was first used in citronellal transformation to menthol followed by in situ reduction of the spent catalyst using the same temperature program as described above and thereafter citral transformation to menthol was started by adjusting the temperature and pressure initially to 70 °C and 20 bar respectively.

The conversion was defined in the current work as follows

$$X = \frac{C_{o,citral} - C_{t,citral}}{C_{o,citral}} * 100\% \qquad (1)$$

The yield is calculated as moles of product i formed divided by the sum of products visible in GC:

$$Y = \frac{n_i}{\sum n_P} * 100\% \qquad (2)$$

The liquid phase mass balance closure is the sum of the masses for the reactant and the products determined by GC analysis.

Stereoselectivity *SS* for menthols is defined as:

$$SS = \frac{y_{Me}}{\sum y_M} * 100\% \qquad (3)$$

where Me is ($\pm$)-menthol and M denotes all menthols.

2.4. Analysis

The liquid samples were taken at different reaction times, and then diluted with cyclohexane. A gas chromatograph an Agilent GC 6890 N equipped with a capillary column DB-1 (30 m x 250 μm x 0.5 μm) and a FID detector was employed. The following temperature program was used: 110–0.4 °C/min - 130–13 °C/min - 270 °C. The temperature of the FID detector was 340 °C. Helium was used as a carrier gas. The products were confirmed with Agilent GC/MS 6890 N/5973 using the same temperature program and the column.

3. Results and discussion

3.1. Catalyst characterization

The physical-chemical properties of synthesized bifunctional Ni/H-Beta-38-sepiolite extruded catalyst were studied by TEM, SEM, XPS, XRD, ICP-OES, N_2 physisorption methods and FTIR spectroscopy.

5 wt% Ni/(H-Beta-38 +sepiolite) extrudates contained 30 wt% a clay sepiolite binder composed of 21 wt% Si, 1 wt% Al, 11 wt% Mg and 0.5 wt% K with Si/Al molar ratio of 16, while the composition of H-Beta-38 zeolite was determined to be as follows: 31.9 wt% Si, 1.7 wt% Al, with the corresponding Si/Al molar ratio of 18 [43].

SEM images of sepiolite show clearly its fibrous structure (Fig. 2a), as has been also reported in the literature [44–46]. The length and width of the fibres is maximally 1150 nm and 15 nm, respectively [46]. According to the literature [47], sepiolite has channels with cross sectional dimensions of 1.06×0.37 nm. H-Beta-38 particles are round-shaped, exhibiting a diameter of ca. 125 nm and a channel structure clearly visible in Fig. 2b.

The powder forms of Ni/(H-Beta-38 +sepiolite) composite and its constituents, sepiolite and NH_4-H-Beta-38, were analyzed by TEM to investigate their nanoscale structure (Fig. 3). Fig. 3a,b demonstrates different pristine nanostructures of needle-shape sepiolite and spherically shaped NH_4-H-Beta-38 that allowed to visualize Ni particles deposited on each material as presented in Fig. 3c,d for the fresh reduced and spent Ni/(H-Beta-38 +sepiolite) extrudates respectively. Rather large Ni particles with the average particle size of 25.5 nm and the median size of 23 nm located both on sepiolite and on the zeolitic phase are visible for the fresh reduced composite catalyst Ni/(H-Beta-38 +sepiolite). After the reaction the nickel average particle size was not significantly changed which was confirmed by XRD data detected size of Ni^0 coherently scattering domain (CSD) 19 nm (see below). According to ICP-OES measurements only minor Ni leaching occurred from the spent catalyst (see below).

A powder X-ray diffraction (XRD) method was applied to study composition and the coherently scattering domain (CSD) of nickel phases in Ni/(H-Beta-38 +sepiolite) extrudates after calcination (Fig. 4) followed by reduction with hydrogen (Fig. 5) and after conversion of citral into menthol (Fig. 6).

The X-ray diffraction pattern of the calcined non-reduced Ni/(H-Beta-38 +sepiolite) extrudates contains only reflexes from the Beta-zeolite (PDF No. 00–056–0487) without any additional lines characteristic for the crystallized nickel-containing phases. This may be due to a highly dispersed state of the nickel compounds (when the crystallite size is less than 2.5 nm). The zeolite structure was shown to be intact after the extrusion, calcination as well as after subsequent impregnation with a nickel precursor followed by its decomposition at 450 °C for 6 h. The X-ray diffraction pattern of the reduced Ni/(H-Beta-38 +sepiolite) fresh extrudates was compared with that of the pristine Beta zeolite (Fig. 5). The X-ray diffraction pattern of the former contains lines from the metallic Ni^0 phase (PDF No. 04–0850, a = b = c = 3.524 Å). The average coherently scattering domain (CSD) of the Ni^0 phase was 23.0 nm indicating possible agglomeration of Ni nanoparticles during the reduction. This is in line with the median particle size of Ni (23 nm) determined by TEM (Fig. 3). The determined lattice value is a = 3.524 Å. The X-ray diffraction pattern of the sample also contains the reflexes of the nickel oxide phase NiO (PDF No. 047–1049, a = b = c = 4.177 Å) with the determined lattice parameters a = b = c = 4.182 Å.
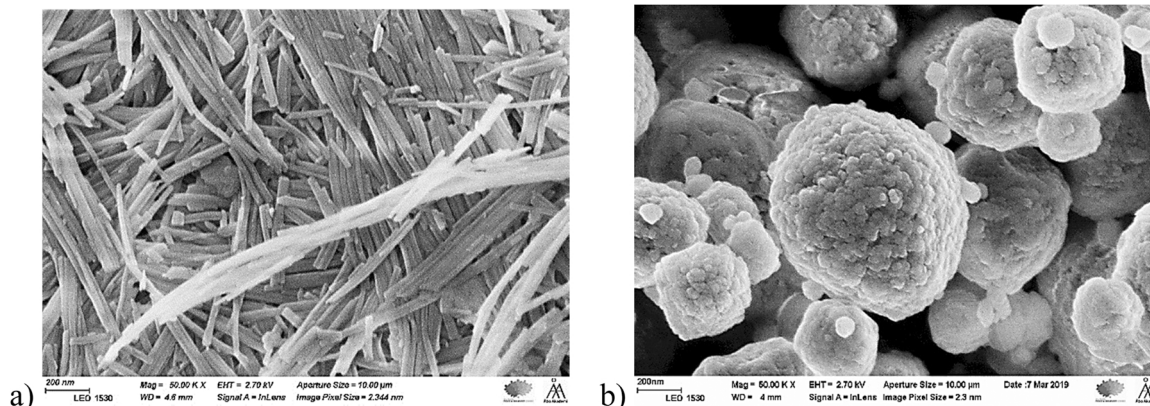

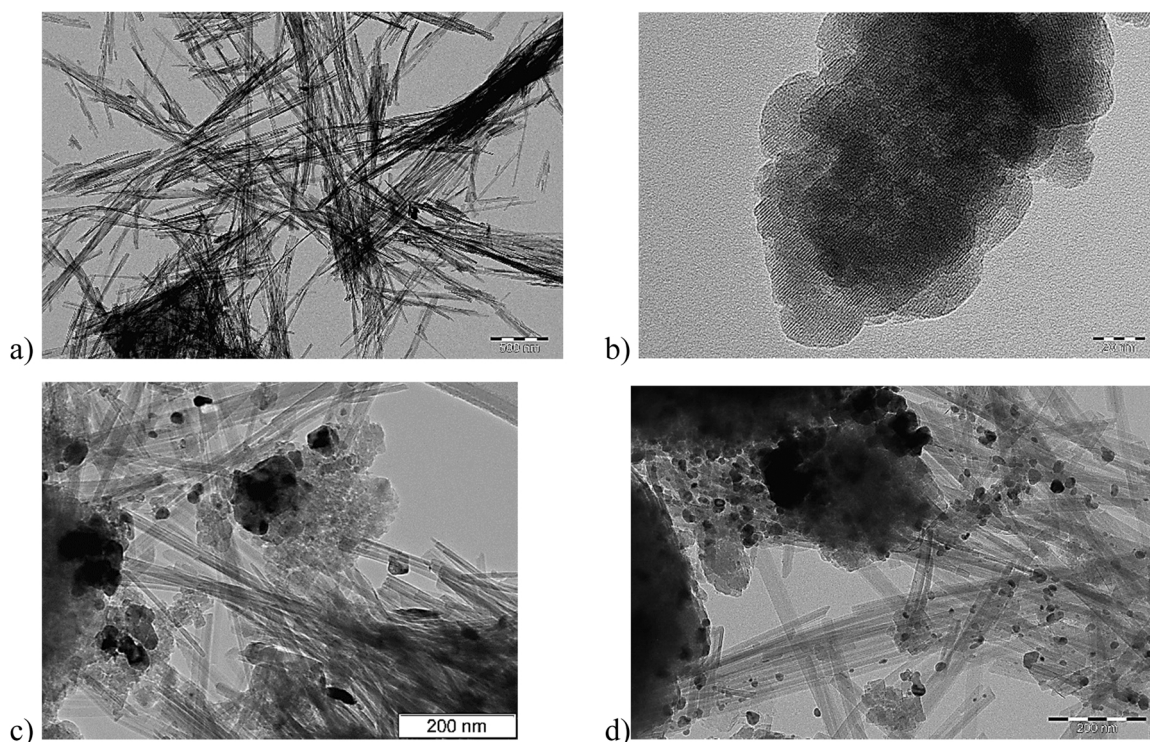**Fig. 2.** SEM images of a) sepiolite and b) H-Beta-38.

Fig. 3. TEM images of a) sepiolite, b) NH$_4$-H-Beta-38, c) fresh reduced Ni/(H-Beta-38 +sepiolite) extrudates, d) spent Ni/(H-Beta-38 +sepiolite) extrudates.

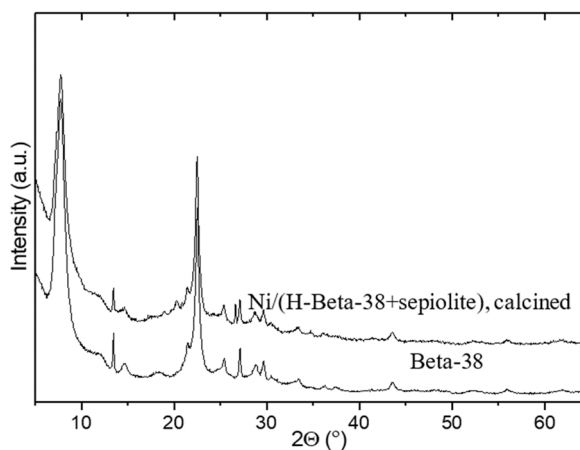**Fig. 4.** XRD patterns of calcined, non-reduced Ni/(H-Beta-38 +sepiolite) extrudates compared to the initial Beta-38 zeolite.

Fig. 5. XRD patterns of the fresh reduced Ni/(H-Beta-38 +sepiolite) extrudates compared to the initial Beta-38 zeolite.

The average CSD of the Ni oxide phase was 10.5 nm. The content of Ni^0 is predominant compared to the oxide phase. The appearance of new additional peaks at 2Θ 10.9, 20.4° indicates that the zeolite underwent minor structural changes. Fig. 6 shows the XRD pattern of the spent Ni/(H-Beta-38 +sepiolite) extrudates compared to the pristine Beta zeolite. Only the metallic Ni^0 phase was identified with the corresponding CSD size equal to 19.0 nm. The determined value of the lattice parameter is a = 3.525 Å. The zeolite underwent some further structural changes during the reaction, which is shown by a decrease in the intensity of the reflexes at 2Θ = 7.7° and 13.4° along with the appearance of lines at 2Θ 10.9° and 20.4° in the fresh reduced catalyst. The areas of these changes are indicated by arrows in Fig. 6.

The N$_2$ physisorption isotherms of the fresh H-Beta-38, fresh and spent Ni/(H-Beta-38 +sepiolite) extrudates, and pristine sepiolite powder as well as the pore size distribution calculated by NLDFT are presented in Fig. 7. The textural properties of sepiolite, H-Beta-38 and those
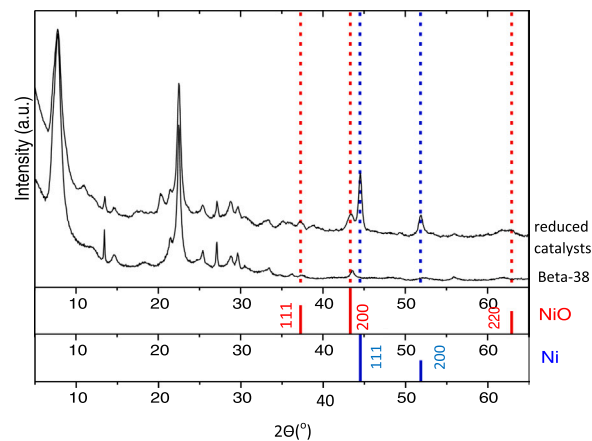
for fresh and spent Ni/(H-Beta-38 +sepiolite) composite studied by N$_2$ low temperature physisorption are presented in Table 2. H-Beta-38 exhibits a large specific surface area and microporosity (V$_\mu$), while sepiolite clay has a relatively low surface area and a large proportion of mesopores (V$_m$) (Fig. 7, Table 2). It has also been reported in the literature that sepiolite possesses in addition to micropores also a large amount of meso- and macropores [46]. The fresh calcined extrudates Ni/(H-Beta-38 +sepiolite) exhibited the specific surface area of 242 m^2/g$_{cat}$ (S$_{BET}$) or of 347 m^2/g$_{cat}$ (S$_{DR}$) calculated by the BET and Dubinin-Radushekevich method, correspondingly, with the ratio between the micro to meso pore volume (V$_\mu$/V$_m$) of 1.1 (Table 2), while sepiolite exhibited in addition to micropores also a large amount of mesopores analogously to the literature [46]. The lower specific surface area of extrudates compared to the expected one as a linear combination of constituents can be related to the chemical interactions between the zeolite and the binder, and an extrusion impact per-se [48,49], while
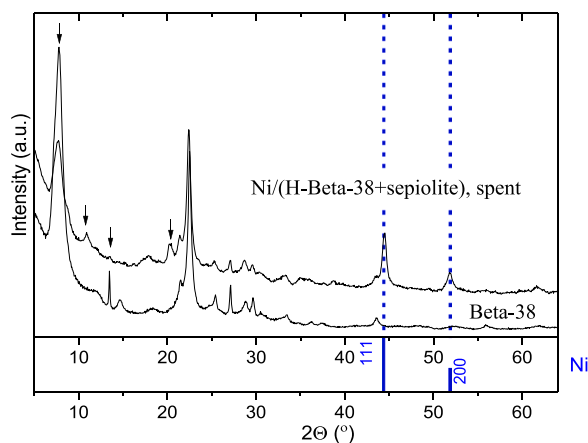
Fig. 6. XRD patterns of the spent Ni/(H-Beta-38 +sepiolite) and the initial Beta-38 zeolite.

deposition of the metal by impregnation further decreased the accessible surface apparently due to a partial pore blocking.

Nickel content in the fresh reduced Ni/(H-Beta-38 +sepiolite) extrudates was 9.4 wt% and only a minor fraction of this loading (ca. 0.04 wt%) was leached out from the spent catalyst according to ICP-OES measurements. This result confirming minor leaching clearly indicates that Ni is strongly bound to the support.

The median pore width according to Fig. 7b and the surface area for the spent Ni/(H-Beta-38 +sepiolite) extrudates was somewhat lower after catalytic experiments with citral and citronellal consequent transformations compared to the fresh catalyst.

The results from the acidity measurements by FTIR with pyridine adsorption/desorption (pyridine-FTIR) show that sepiolite has a low acidity and 8.2 fold more Lewis than Brønsted acid sites (LAS and BAS, respectively) (Table 3). Furthermore, it does not contain LAS and BAS strong acid sites. On the other hand, Ni/(H-Beta-38 +sepiolite) contained strong Brønsted and Lewis acid sites and the ratio between Brønsted to Lewis acid sites (BAS/LAS) concentration was 5 fold higher than that for sepiolite. The acidity of the parent H-Beta-38 was, however, high and the zeolite contained also a high amount of strong Brønsted acid sites. The amount of Brønsted acid sites in the composite catalyst was rather low, while the metal deposition increased the concentration of Lewis acid sites. The theoretical value of the Brønsted acidity for metal-free non-interacting mechanical H-Beta-38 +sepiolite mixture was ca. 2.3 fold higher and 5.5 fold lower than for Ni/(H-Beta-38 +sepiolite) extrudates in terms of Brønsted and Lewis acid sites,

respectively. The mass ratio of H-Beta-38 to sepiolite in Ni/(H-Beta-38 +sepiolite) was also 2.3, which is in line with the total Brønsted acidity decrease in Ni/(H-Beta-38 +sepiolite) in comparison to the metal free extrudates. However, incorporation of Ni resulted in a significant decrease of the amount of strong Brønsted acid sites indicating predominate deposition of Ni species on these sites, being in line with the literature [50].

Table 2
The textural properties of different supports and the extrudates.[a]

Sample	S_{BET}	S_{DR}	V	V_μ	V_m	V_μ/V_m
	m^2/g	m^2/g	cm^3/g	cm^3/g	cm^3/g	-
H-Beta-38, powder	n.a.	590	0.31	0.23	0.08	2.9
Sepiolite powder (ref.[38])	135	141	0.31	0.05	0.26	0.2
70 wt% H-Beta-38 + 30 wt% sepiolite, theoretical values as linear combinations	n.a.	453	0.31	0.18	0.13	2.1
70 wt% H-Beta-38 + 30 wt% sepiolite	235	368	0.18			1.5
Ni/(H-Beta-38 +sepiolite), fresh extrudates	242	347	0.26	0.14	0.12	1.1
Ni/(H-Beta-38 +sepiolite), spent extrudates	162	234	0.20	0.10	0.10	0.9

[a] A – specific surface area (BET: Brunauer-Emmett-Teller, DR: Dubinin-Radushkevich), V – pore volume (m: meso, μ: micro) calculated by NLDFT.

Table 3
Acidity of sepiolite and Ni/(H-Beta-38 +sepiolite) catalyst determined by pyridine-FTIR.[a]

Sample	BAS (μmol g^{-1})				LAS (μmol g^{-1})				BAS/LAS
	w	m	s	$\sum$	w	m	s	$\sum$	
H-Beta-38 (ref. [35])	17	40	221	278	19	9	2	31	9.0
Sepiolite (ref.[38])	6	2	0	8	55	11	0	66	0.12
70 wt% H-Beta-38 + 30 wt% sepiolite, theoretical value	14	29	155	198	30	10	1	41	4.8
Ni/(H-Beta-38 +sepiolite)	26	39	21	86	90	30	22	230	0.60

[a] Brønsted (BAS) and Lewis acid sites (LAS) were measured by pyridine adsorption-desorption at 250 °C, 350 °C and 450 °C, corresponding to weak (w, data at 250 °C minus data at 350 °C), medium (m, data at 350 °C minus data at 450 °C) and strong (s, data at 450 °C) acid sites, respectively.
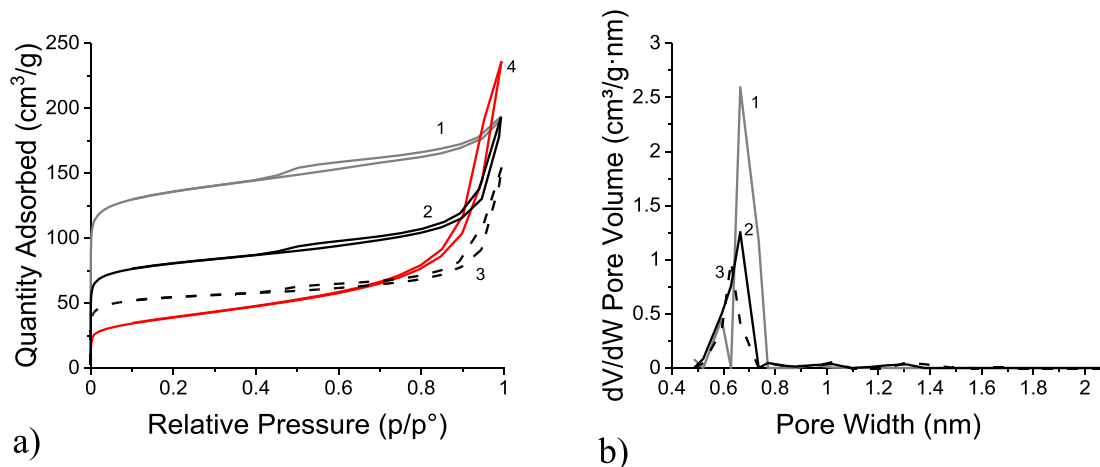

Fig. 7. a) Isotherms and b) the pore size distribution by DFT. Notation: 1 - fresh H-Beta-38 powder, 2 - fresh (Ni/H-Beta-38 +sepiolite) extrudates, 3 - spent (Ni/H-Beta-38 +sepiolite) extrudates, 4 – pristine sepiolite powder.

3.2. Catalytic results

3.2.1. Citronellal transformation

The trickle bed reactor is operating under mass transfer limitations [23,25], while in the batch reactor the kinetic regime was maintained because of a small particle size and efficient stirring [33]. The initial reaction rate for citronellal transformation over extrudates was calculated in the current work at 60 min TOS to be $2.8 \cdot 10^{-7}$ mol/s·g_{cat} with the initial citronellal concentration of 0.086 M at 70 °C under 20 bar total pressure, when using the following equation [25]:

$$r_E = \frac{\Delta \dot{n}}{m_{cat}} \quad \left[\frac{mol}{s.g} \right] \tag{4}$$

This value is only 42–57% of the initial rates obtained with Ru-MCM-41 at 70 °C under 10 bar hydrogen in ref. [20]. Citronellal conversion decreased initially until 150 min TOS, thereafter it remained the same (Fig. 8a), although the pressure was increased from 20 bar after 150 min to 29 bar. Furthermore, citronellal conversion decreased after 240 min TOS when the pressure was decreased to 10 bar. At the same time the liquid phase mass balance closure, increased from 32% at 95 min TOS to 70% at 270 min TOS analogously to the results in ref. [24] where the liquid phase mass balance closure increased characterizing the reactor dynamics. The mass balance closure increased apparently because some part of the reactant and products is initially strongly adsorbed on the catalyst surface being desorbed thereafter with increasing TOS.

The product distribution in citronellal transformation to menthol is shown in Fig. 8b. The main products initially were defunctionalized products (DFP) such as *p*-menthanes formed via dehydration of menthols analogously to ref. [24]. It should be pointed out, however, that in citronellal transformation to menthols over mild acidic Ru-MCM-41 maximally 2.2% of defunctionalized products were formed, while in the current case with a highly acidic Ni/(H-Beta-38 +sepiolite) the maximum yield of DFPs was 31%. The yield of DFP decreased, however, with increasing TOS due to catalyst deactivation and at the same time the yield of menthol increased. Noteworthy that even at 280 min TOS under 10 bar the highest menthol yield was 43%. In addition stereoselectivity to (-)-menthol was rather constant, in the range of 71–76% with increasing TOS (Fig. 8b). It can also be observed that when DFP concentration decreased with increasing TOS, the yield of acyclic hydrogenation products increased (Fig. 8c). Furthermore, it is important to note that the yield of 3,7-dimethyloctanol increased continuously with increasing TOS and the opposite was found for citronellol which is an intermediate product (Fig. 8c). This result indicates together with increasing yield of menthols that hydrogenation of citronellol and isopulegols proceeded efficiently, while the undesired hydrogenolysis reaction was suppressed.
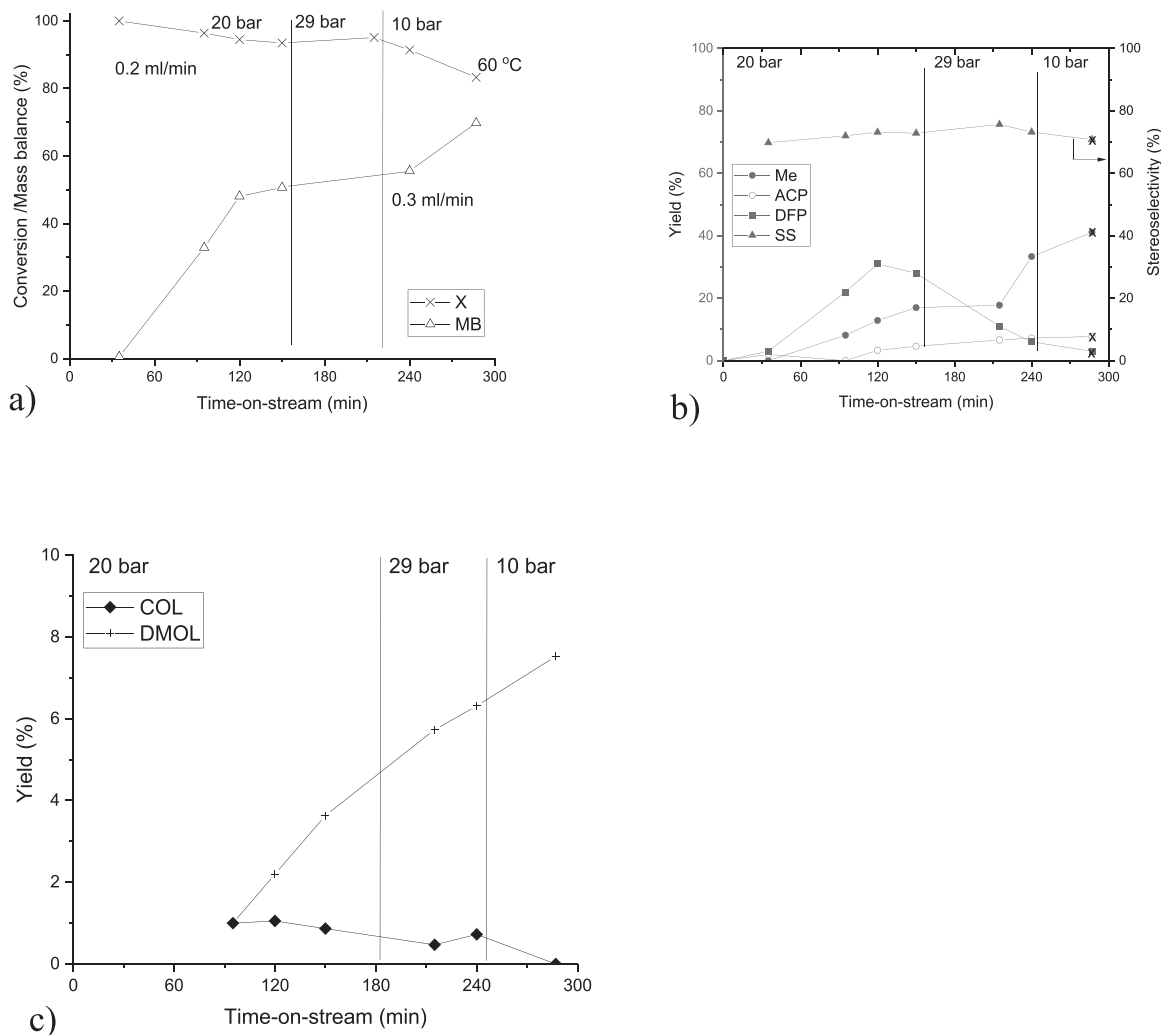

Fig. 8. Citronellal transformations as a function of time-on-stream: a) Citronellal conversion (X) and liquid phase mass balance closure (*MB*), b) yield of menthols (Me), acyclic hydrogenation products (ACP) and defunctionalized products (DFP) and stereoselectivity in menthols (SS), c) yield of citronellol (CAL) and 3,7-dimethyloctanol (DMOL). Notation: Citronellal transformation was performed at 70 °C up to 240 min TOS after which temperature was adjusted to 60 °C. Reaction conditions: citronellal in cyclohexane solution 0.086 M, 1 g catalyst, flow rate of the citronellal solution 0.4 mL/min; H_2 flow rate 100 mL/min.

3.2.2. Citral transformation

In the citral transformation the initial reaction rate over the same catalyst calculated from Eq. (1) was $4.1 \cdot 10^{-7}$ mol/s·g_{cat} with the initial citral concentration of 0.086 M at 70 °C under 20 bar total pressure. As a comparison the initial rate of citral transformations was in the same range over Ru-MCM-41 in a trickle bed reactor at 70 °C under 10 bar total pressure [37], while in the batch reactor ca. 51 fold higher rate was obtained over a powder catalyst. In the current work, the main focus was exclusively on the catalyst behavior in the continuous reactor.

Conversion of citral was maximally 95% under 20 bar hydrogen at 70 °C over Ni/(H-Beta-38 +sepiolite), however, it declined during the following 2 h time-on-stream to 88% (Fig. 8a). Typically, in citral
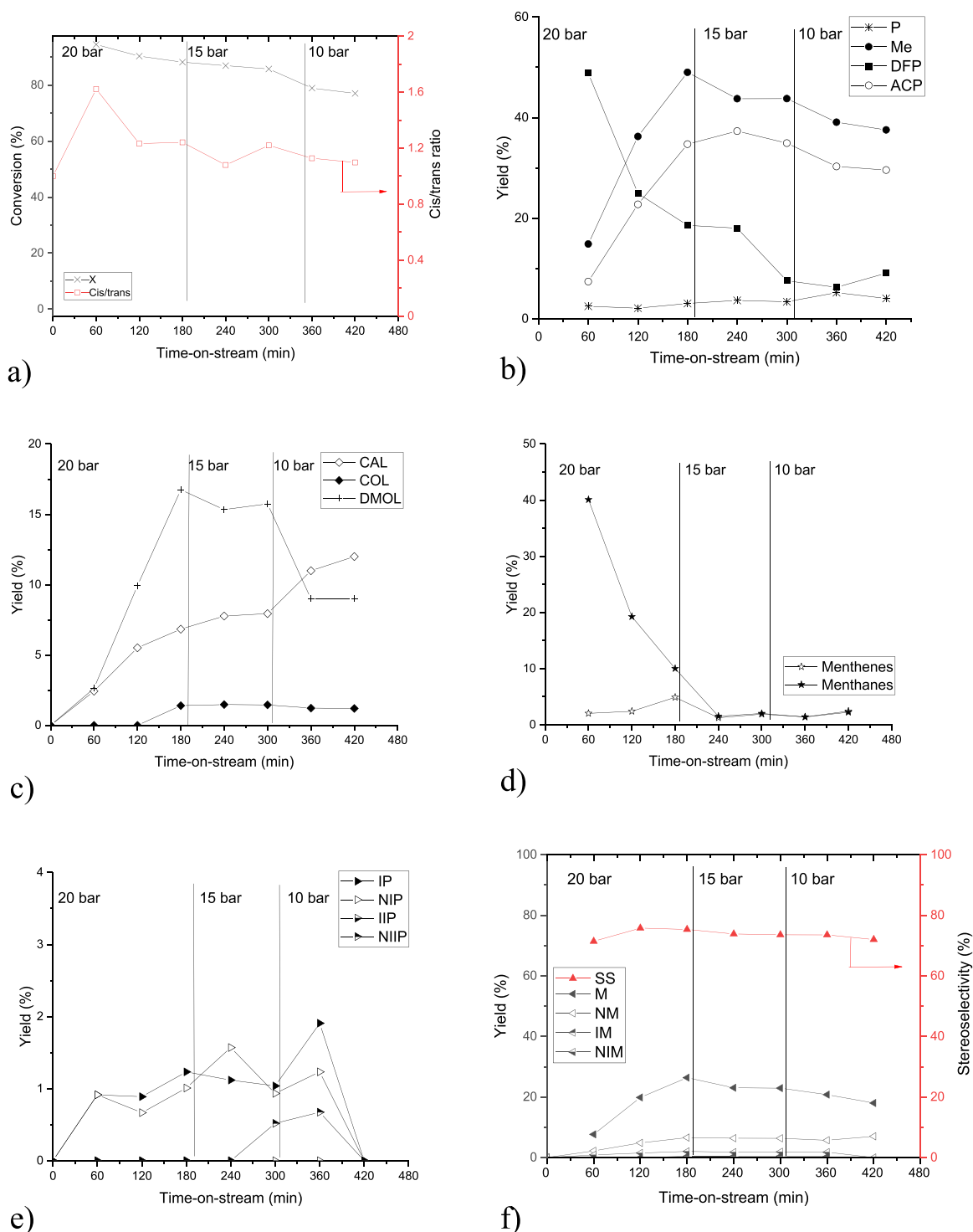

Fig. 9. Transformation of citral as a function of time-on-stream: a) citral conversion and cis/trans ratio, b) yield of menthols (Me), pulegols (P), acyclic hydrogenation products (ACP) and defunctionalized products (DFP), c) citronellal (CAL), citronellol (COL) and 3,7-dimethyloctanol (DMOL), d) yield of menthenes (products 9–11) and menthanes (product 14), e) isopulegol (IP), neoisopulegol (NIP), isoisopulegol (IIP) and neoisoisopulegol (NIIP) and f) menthol (M), neomenthol (NM), isomenthol (IM) and neoisomenthol (NIM) and stereoselectivity to menthol (SS). Reaction conditions: citral in cyclohexane solution 0.086 M, 70 °C, 1 g catalyst, flow rate of the citral solution 0.4 mL/min; H_2 flow rate 100 mL/min. The residence time was 11.5 min.

transformations to menthols the citral conversion is linearly dependent on hydrogen pressure in a batch reactor [29]. In the current case, the reactor dynamics is slow showing that when pressure was decreased to 15 bar, citral conversion did not drop as expected. On the other hand, in this case, citral conversion decreased with the same rate as under 20 bar. Finally, under 10 bar hydrogen a larger drop in citral conversion was observed. Compared with the current results, continuous citral transformation over Ni-supported on mesoporous aluminosilicate with the sepiolite binder demonstrated at the same temperature of 70 °C complete conversion of the substrate during the first 8 h TOS [40]. When, however, changing the pressure from the initial 10–5 bar and then returning back to 10 bar at TOS 19 h, it could also be clearly seen that the steady state was not observed due to catalyst deactivation [40]. When comparing the properties of 5 wt% Ni/MAS (mesoporous aluminosilicate) [40] with those for Ni/(H-Beta-38 +sepiolite), the former one exhibited 12 nm Ni particles and very mild acidity (total concentration of acid sites was 65 mmol/g$_{cat}$), while in the current case the average Ni particle size and total acidity of Ni/(H-Beta-38 +sepiolite) were 25.5 nm and 316 mmol/g$_{cat}$, respectively. These differences in acidity and worse metal dispersion resulted in more extensive deactivation in the case of Ni/(H-Beta-38 +sepiolite).

The *cis/trans* ratio in the initial citral feed was 1. At 1 h TOS it was increased to 1.6 indicating that *cis*-citral was reacting much slower than *trans*-citral over an acidic catalyst in the presence of diffusional limitations. This ratio, however, decreased when TOS reached 1.1–1.2 h and thus *cis*-citral exhibited higher reactivity compared to *trans*-citral analogously to the previous reports on citral transformations in a batch reactor at 70 °C under 10 bar over powder Ni/H-MCM-41 catalyst [33].

Typically in one-pot citral transformations to menthol (compound 8) the challenge is to diminish the competing hydrogenation reactions forming citronellol (compound 4), and 3,7-dimethyloctanol (compound 5) as well as dehydration of menthols, forming menthenes (compounds 9–11) as primary products and hydrogenation products, i.e. menthanes (compound 14), as well as dehydrogenation to menthadienes (limonene, compound 12) and *p*-cymene (compound 13) (Fig. 1) [33]. Due to a high total acidity of Ni/(H-Beta-38 +sepiolite) catalyst (316 μmol/g, Table 3) the main products at 1 h TOS were defunctionalized products, such as 1-methyl-4-(1-methylethyl)-trans-cyclohexane and the corresponding *cis*-cyclohexane (Fig. 9b). In the current case, initially 1-methyl-4-(1-methylethyl)-trans-cyclohexene was formed via menthol dehydration, which occurred in the presence of an acidic catalyst. When menthol is dehydrated over an acidic catalyst, a carbocation is formed via a hybrid shift when the formed water is cleaved. Thereafter, an ethylenic double bond is formed between the carbon atoms adjacent to the carbocation. The formed menthenes were subsequently rapidly hydrogenated giving a large amount of menthanes with the yield of ca. 40% already after 1 h TOS under 20 bar total pressure (Fig. 9d). With increasing TOS the yield of defunctionalized products decreased rapidly and the yield of defunctionalized products at the end of the experiment was below 10% (Fig. 9b). Catalysts with high Brønsted acidity typically promote alcohol dehydration as observed in the literature [51]. For example a large amount of styrene, a dehydration product from 1-phenylethanol, was formed in its liquid phase dehydration at 90 °C over a highly Brønsted acidic H$_3$PW$_{12}$O$_{40}$/SiO$_2$. When comparing the current results with Ni/(H-Beta-38 +sepiolite) performed in a trickle bed reactor at 70 °C with those performed in a batch reactor using 3 wt% Ni/Beta with the SiO$_2$/Al$_2$O$_3$ molar ratio of 25 and the ratio of Brønsted to Lewis acid sites of 1, the latter one gave maximally 81% menthol yield [27]. In the current case, the maximum menthol yield was 49% over the catalyst with the Brønsted to Lewis acid site ratio of 0.6 (BAS/LAS ratio). It should also be pointed out that in the literature [31] the highest menthol yield was 94% obtained in a batch reactor over a mildly acidic Ni-MCM-41 in a powder form with the BAS/LAS ratio of the support being 0.33. Interestingly, the BAS/LAS ratio in 5 wt%/Ni/MAS (mesoporous alumino silicate) was high, 0.85, however, low selectivity to DFP products was obtained in citral transformation to menthols indicating

that it is not only the BAS/LAS ratio, but also the total acidity, which is prerequisite for obtaining high menthol yields [40].

Menthols were the main products with the yield of 36% already after 2 h TOS (Fig. 9b) and their amount reached a maximum level of 49% at 3 h TOS under 20 bar total pressure. At a lower total pressure, 15 bar, menthol yield remained constant corresponding to the yield of 44%, while it declined to 38% under 10 bar at 2 h TOS. Vajglova et al. reported that Ru-MCM-41 gave only 6% menthols in citral transformations at 70 °C under 10 bar total pressure in the same reactor [37] indicating that metal selection is crucial for selective one-pot synthesis of menthol from citral. In addition, the highest yield of menthols reported in the open literature for a trickle bed reactor with extrudates was obtained in [40] being maximally 75% with a mildly acidic 5 wt% Ni/MAS.

Stereoselectivity to menthol remained also relatively constant during the whole experiment (Fig. 9f), being ca. 72–74%. As a comparison, lower hydrogen pressures favored menthol formation over Zr-Beta-15 wt% Ni-MCM-41 at 90 °C in a batch reactor and the maximum diastereoselectivity to menthol was 94% under 20 bar at 80 °C in tert-butanol [29]. The role of Zr was to provide intraporous Lewis acid sites, which promote stereoselective cyclisation of citronellal [29]. Despite a high amount of Lewis acid sites in Ni/(H-Beta-38 +sepiolite) dehydration of menthol was also efficient due to the presence of strong Brønsted acid sites.

The yield of the formed acyclic hydrogenation products was slightly lower than that of menthols (Fig. 9b), but it followed the same kinetic profile as menthol showing a maximum yield at 4 h TOS at 15 bar total pressure. Parallel formation of menthols and acyclic hydrogenation products occurred during the first 3 h TOS under 20 bar total pressure (Fig. 10b). The concentration of menthols and acyclic hydrogenation products decreased, however, after 3 h and 4 h TOS, respectively, when the pressure was lowered to 15 and 10 bar (Fig. 10b). The yields of the intermediate products, pulegols, remained low due to their fast hydrogenation to menthols. Their yield was below 5% during the whole experiment (Fig. 9b,e). These results show that Ni/(H-Beta-38 +sepiolite) extrudates were active in hydrogenating pulegols to menthols even if the Ni particle size was rather large.

The detailed analysis of different hydrogenation products formation shows that the undesired hydrogenation of citronellal occurred also rapidly to 3,7-dimethyloctanol, which was the main hydrogenation product during the first 360 min TOS, after which the main product was citronellal (Fig. 9c). The reason for this is that hydrogenation rate decreased with decreasing hydrogen partial pressure at 240 min and at 300 min. Note that the first order hydrogen dependence for citral hydrogenation over Ni/Cr$_2$O$_3$ was observed in a batch reactor [52]. This result indicates that the consecutive hydrogenation of citronellal has been substantially suppressed. It was also interesting to observe, that after prolonged TOS in the presence of a rather high concentration of citronellal dimeric ether of citronellal was not observed, while it was typically formed in one-pot synthesis of menthols in a continuous reactor starting from citronellal over Ru- and Pt-Beta zeolites [25]. Furthermore, hydrogenation of citronellol to 3,7-dimethyloctanol occurred initially very rapidly, because no citronellol was present in the product mixture during 120 min TOS under 20 bar. No nerol and geraniol were formed and only traces of 3,7-dimethyloctanal were observed. The yield of citronellol remained stable corresponding to the yield of ca. 2% (Fig. 9c).

Selectivity changes for different product types are visible in Fig. 10 a. It can be seen initially selectivity for both acyclic hydrogenation products (ACP) and menthols were increasing with increasing TOS and decreasing conversion, while the most prominent products were DFPs. Pulegols were typically rapidly reacting further and exhibited low selectivity. However, at 300 min TOS the selectivity to ACP dropped substantially indicating catalyst deactivation. It was also observed that selectivity to the primary product, citronellal continuously increased while that for 3,7-dimethyloctanol decreased with increasing time-on-stream (not depicted here). The current result differs from that
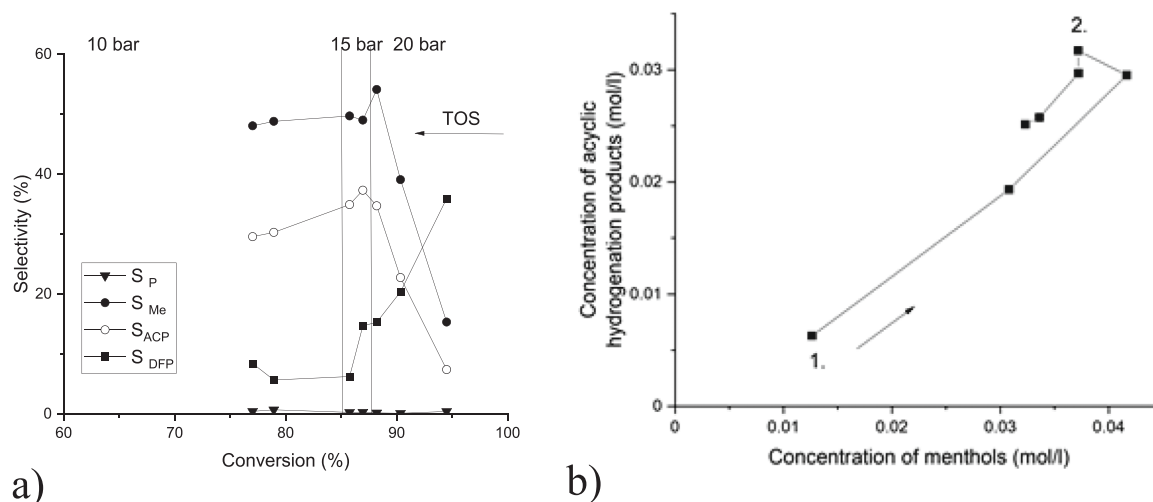
Fig. 10. Transformation of citral in a continuous flow reactor: a) selectivity to the main products as a function of conversion, notation: pulegols (P), menthols (Me), acyclic hydrogenation products (ACP) and defunctionalized products (DFP), observe that TOS increases with decreasing conversion, b) concentration of hydrogenation products versus the concentration of menthols in citral transformations. Notation: 1. TOS of 60 min, 2. TOS of 240 min, TOS increases with the arrow direction. Conditions: Ni/(H-Beta-38 +sepiolite) extrudates 1 g, citral in cyclohexane solution 0.086 M, 70 °C, flow rate of the citral solution 0.4 mL/min; H_2 flow rate 100 mL/min. The residence time was 11.5 min.

published in [40], because menthol selectivity decreased with increasing TOS when using 5 wt% Ni/MAS catalyst, while in the current case a maximum selectivity to menthols was obtained. This difference can be attributed to higher acidity of Ni/(Beta-38 +sepiolite) compared to that of 5 wt% Ni/MAS.

It should be concluded that despite high menthol yields exceeding literature values for the continuous one-pot transformations of citral, further work is required to optimize Ni loading and catalyst acidity to diminish the competing side reactions, i.e. hydrogenation of citronellal and dehydration of menthol.

4. Conclusions

One-pot synthesis of menthols from citronellal and citral was demonstrated in a trickle bed reactor over nickel supported on extrudates comprising H-Beta-38 and sepiolite as a binder. The composite catalyst exhibited both Brønsted and Lewis acid sites with their ratio of 0.60 and nickel clusters of ca. 23 nm. The fresh reduced catalyst was tested in citronellal transformation to menthol in cyclohexane giving 53% yield of menthols and 70% stereoselectivity at 10 bar total pressure at 60 °C after 270 min time-on-stream in a trickle bed reactor. Thereafter, the catalyst was reduced in situ at 350 °C for 120 min prior to citral transformation. In citral transformation, the main products were initially p-menthanes formed via dehydration of menthol, which occurred due to high Brønsted acidity. The highest menthol yield starting from citral was 49% with stereoselectivity 72–74% was obtained at 180 min time-on-stream at 70 °C under 20 bar total pressure. Conversion of citral decreased with increasing time-on-stream due to catalyst deactivation and at the same time selectivity to menthols increased, which was related to suppression of menthols dehydration giving initially menthanes as the main product. Deactivation with increasing time-on-stream was also clearly visible from increasing selectivity of citronellal.

CRediT authorship contribution statement

Irina Simakova: Investigation, Supervision, Visualization, Writing – review and editing. **Päivi Mäki-Arvela:** Conceptualization, Writing – original draft. **Mark Martinez-Klimov:** Investigation. **Joseph Muller:** Investigation. **Zuzana Vajglová:** Investigation. **Markus Peurla:** Investigation. **Kari Eränen:** Supervision. **Dmitry Yu. Murzin:** Conceptualization, Writing – review & editing, Supervision, Project administration.

Declaration of Competing Interest

The authors declare that they have no known competing financial interests or personal relationships that could have appeared to influence the work reported in this paper.

References

[1] B.M. Lawrence. B. M. Lawrence, Mint: The Genus Mentha, CRC Press, Boca Raton, 2007, p. 2006.
[2] Sayo, N.and Matsumoto, T. Method for Producing L-Menthol. US6342644B1, 2002.
[3] J. Lawless, The Encyclopedia of Essential Oils: A Complete Guide to the Use of Aromatics in Aromatherapy, Herbalism, Health and Well-Being (Health Workbooks), second ed., HarperCollins Publishers Limited, Glasgow, 1992.
[4] A. Chauvel, B. Delmon, W.F. Holderich, Appl. Catal. A 115 (1994) 173–217.
[5] P. Mäki-Arvela, N. Kumar, V. Nieminen, R. Joholm, T. Salmi, D.Y. Murzin, J. Catal. 225 (2004) 155–169.
[6] Z. Vajglova, N. Kumar, P. Maki-Arvela, K. Eranen, M. Peurla, L. Hupa, D.Y. Murzin, Org. Proc. Res. Dev. 23 (11) (2019) 2456–2463.
[7] Z. Vajglová, N. Kumar, P. Mäki-Arvela, K. Eränen, M. Peurla, L. Hupa, M. Nurmi, M. Toivakka, D.Y. Murzin, Ind. Eng. Chem. Res. 58 (39) (2019) 18084–18096.
[8] C.B. Cortes, V.T. Galvan, S.S. Pedro, T.V. Garcia, Catal. Today 172 (2011) 21–26.
[9] I.B. Adilina, R. Pertiwi, A. Sulaswatty, Biopropal Ind. 6 (1) (2015) 1–6.
[10] F. Neațu, S. Coman, V.I. Pârvulescu, G. Poncelet, D. De Vos, P. Jacobs, Top. Catal. 52 (9) (2009) 1292–1300.
[11] J. Plößer, M. Lucas, P. Claus, J. Catal. 320 (2014) 189–197.
[12] F.G. Cirujano, F.X. Llabrés, I. Xamena, A. Corma, Dalton Trans. 41 (14) (2012) 4249–4254.
[13] P. Mertens, F. Verpoort, A.N. Parvulescu, D. De Vos, J. Catal. 243 (1) (2006) 7–13.
[14] C. Milone, C. Gangemi, G. Neri, A. Pistone, S. Galvagno, Appl. Cat. A Gen. 199 (2) (2000) 239–244.

[15] C.B. Cortés, V.T. Galván, S.S. Pedro, T.V. García, Catal. Today 172 (1) (2011) 21–26.

[16] J. Ten Dam, A. Ramanathan, K. Djanashvili, F. Kapteijn, U. Hanefeld, RSC Adv. 7 (20) (2017) 12041–12053.

[17] Y. Nie, W. Niah, S. Jaenicke, G.K. Chuah, J. Catal. 248 (1) (2007) 1–10.

[18] J. Plößer, M. Lucas, J. Wärnå, T. Salmi, D.Y. Murzin, P. Claus, Org. Proc. Res. Dev, 20, 2016, pp. 1647–1653.

[19] A. Negoi, S. Wuttke, E. Kemnitz, D. Macovei, V.I. Parvulescu, C.M. Teodorescu, S. M. Coman, Angew. Chem. Int. Ed. 49 (44) (2010) 8134–8138.

[20] J. Plößer, F. Dedeaga, M. Lucas, P. Claus, Appl. Cat. A Gen. 516 (2016) 100–108.

[21] A.M. Balu, J.M. Campelo, R. Luque, A.A. Romero, Org. Biomol. Chem. 8 (12) (2010) 2845–2849.

[22] F. Iosif, S. Coman, V. Pàrvulescu, P. Grange, S. Delsarte, D. De Vos, P. Jacobs, Chem. Comm. 11 (2004) 1292–1293.

[23] K.A. Silva Rocha, P.A. Robles-Dutenhefner, E.M. Sousa, E.F. Kozhevnikova, I. V. Kozhevnikov, E.V. Gusevskaya, Appl. Cat. A Gen. 317 (2) (2007) 171–174.

[24] A. Zuliani, C.M. Cova, R. Manno, V. Sebastian, A.A. Romero, R. Luque, Green. Chem. 22 (2) (2020) 379–387.

[25] M. Azkaar, P. Mäki-Arvela, Z. Vajglova, V. Fedorov, N. Kumar, L. Hupa, J. Hemming, M. Peurla, A. Aho, D.Y. Murzin, Reac. Chem. Eng. 4 (2019) 2156–2169.

[26] Z. Vajglová, N. Kumar, M. Peurla, K. Eränen, P. Mäki-Arvela, D.Y. Murzin, Catal. Sci. Tech. 10 (23) (2020) 8108–8119.

[27] A.F. Trasarti, A.J. Marchi, C.R. Apesteguia, J. Catal. 224 (2004) 484–488.

[28] O. Muraza, E.V. Rebrov, P. Mäki-Arvela, N. Kumar, M.H.J.M. de Croon, D. Y. Murzin, J.C. Schouten, Sci. Centr Asia 1 (2010) 30–38.

[29] Y.T. Nie, S. Jaenicke, G.K. Chuah, Chem. Eur. J. 15 (2009) 1991–1999.

[30] A. Negoi, K. Teinz, E. Kemnitz, S. Wuttke, V.I. Parvulescu, S.M. Coman, Top. Catal. 55 (2012) 680–687.

[31] A.F. Trasarti, A.J. Marchi, C.R. Apesteguia, J. Catal. 247 (2007) 155–165.

[32] A.K. Shah, G. Maitlo, A.A. Shah, I.A. Channa, G.A. Kandhro, H.A. Maitlo, U. H. Bhatti, A. Shah, A.Q. Memon, A.S. Jatoi, Y.H. Park, Reac. Kinet. Mech. Catal. 128 (2019) 917–934.

[33] P. Mäki-Arvela, N. Kumar, D. Kubička, A. Nasir, T. Heikkilä, V.P. Lehto, D. Y. Murzin, J. Mol. Cat. A (2005) 72–81.

[34] I.V. Deliy, I.G. Danielova, I.L. Simakova, F. Zaccheria, N. Ravasio, R. Psaro, Chem. Ind. 123 (2009) 87–92.

[35] P. Virtanen, T.O. Salmi, J.P. Mikkola, Top. Catal. 53 (2010) 1096–1103.

[36] 2012 Worz, Nicolai W.örz Virtanen, 2011 Jürgen Arras, Claus Peter, Appl. Catal. A Gen. 391 (2011) 319–324.

[37] Z. Vajglová, P. Mäki-Arvela, K. Eränen, N. Kumar, M. Peurla, D.Y. Murzin, Catal. Sci. Technol. 11 (2021) 2873–2884.

[38] Z. Vajglová, M. Navas, P. Mäki-Arvela, K. Eränen, N. Kumar, M. Peurla, D. Y. Murzin, Chem. Eng. J. 429 (2022) 132190.

[39] D.A. McKeown, J.E. Post, E.S. Etz, Clays Clay Miner. 50 (2002) 667–680.

[40] I. Simakova, Z. Vajglová, P. Mäki-Arvela, K. Eränen, L. Hupa, M. Peurla, E. Mäkilä, J. Wärnå, D. Yu, Org. Proc. Res. Dev. 26 (2022) 387–403.

[41] R. Suerz, K. Eränen, N. Kumar, J. Wärnå, V. Russo, M. Peurla, A. Aho, D.Y. Murzin, T. Salmi, Chem. Eng. Sci. 229 (2021) 116030.

[42] C.A. Emeis, J. Catal. 141 (1993) 347–354.

[43] M. Thommes, K. Kaneko, A.V. Neimark, J.P. Olivier, F. Rodriguez-Reinoso, J. Rouquerol, K.S. Sing, Pure Appl. Chem. 87 (2015) 1051–1069.

[44] M. Önal, H. Yilmaz, Y. Sarikaya, Turk. Clays Clay Miner. 56 (2008) 511–519.

[45] E. Sabah, M.S. Celik, J. Am. Oil Chem. Soc. 82 (2005) 911–916.

[46] Z. Vajglová, I.L. Simakova, K. Eränen, P. Mäki-Arvela, N. Kumar, M. Peurla, S. Tolvanen, A. Efimov, L. Hupa, J. Peltonen, D. Yu. Murzin, Appl. Catal. A Gen. 629 (2021) 118426.

[47] S. Argast, Clays Clay Miner. 37 (1989) 371–376.

[48] Z. Vajglova, N. Kumar, M. Peurla, J. Peltonen, I. Heinmaa, D.Y. Murzin, Catal. Sci. Technol. 8 (2018) 6150–6162.

[49] Z. Vajglova, N. Kumar, M. Peutia, L. Hupa, K. Semikin, D.A. Sladkoyskiy, D. Y. Murzin, Ind. Eng. Chem. Res. 58 (2019) 10875–10885.

[50] D. Kubicka, N. Kumar, T. Venalainen, H. Karhu, I. Kubickova, H. Osterholm, D. Y. Murzin, J. Phys. Chem. B 110 (2006) 4937–4946.

[51] N.M. Bertero, A.F. Trasarti, C.R. Apesteguia, A.J. Marchi, Appl. Cat. A Gen. 458 (2013) 28–38.

[52] U. Syunbayev, D.K. Churina, G.Y. Yergaziyeva, N.A. Assanov, K.K. Kalihanov, Int. J. Chem. Eng. Appl. 7 (2016) 133–137.